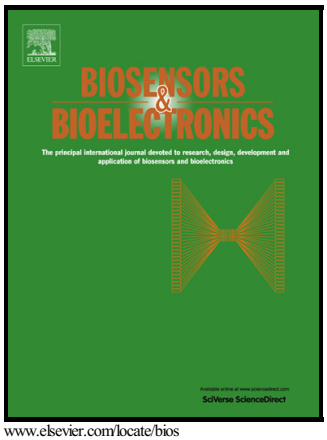

www.elsevier.com/locate/bios

An ultrasensitive DNA biosensor based on covalent immobilization of probe DNA on fern leaf-like α-Fe2O3 and chitosan Hybrid film using terephthalaldehyde as arm-linker

Biyan Xu, Delun Zheng, Weiwei Qiu, Feng Gao, Shaoxiong Jiang, Qingxiang Wang

PII: S0956-5663(15)30111-1
DOI: http://dx.doi.org/10.1016/j.bios.2015.05.015
Reference: BIOS7677

To appear in: *Biosensors and Bioelectronic*

Received date: 10 February 2015
Revised date: 23 April 2015
Accepted date: 6 May 2015

Cite this article as: Biyan Xu, Delun Zheng, Weiwei Qiu, Feng Gao, Shaoxiong Jiang and Qingxiang Wang, An ultrasensitive DNA biosensor based on covalent immobilization of probe DNA on fern leaf-like α-Fe2O3 and chitosan Hybrid film using terephthalaldehyde as arm-linker, *Biosensors and Bioelectronic,* http://dx.doi.org/10.1016/j.bios.2015.05.015

An ultrasensitive DNA biosensor based on covalent immobilization of probe DNA on fern leaf-like α-Fe_2O_3 and chitosan hybrid film using terephthalaldehyde as arm-linker

Biyan Xu, Delun Zheng, Weiwei Qiu, Feng Gao, Shaoxiong Jiang, Qingxiang Wang*

a. College of Chemistry and Environment, Fujian Province Key Laboratory of Morden Analytical Science and Separation Technology, Minnan Normal University, Zhangzhou,363000, P. R. China

b. Department of Natural Sciences, Shantou Polytechnic, Shantou, 515078, China

Submitted to Biosensors and Bioelectronics

*Author for correspondence Prof. Qingxiang Wang, Tel: +86-596-2591445; Fax: +86-596-2520035;

E-mail: axiang236@126.com.

Abstract

In this work, a novel electrochemical DNA biosensor has been developed based on the hybrid film of fern leaf-like α-Fe_2O_3 microparticles and chitosan (CS). The fern leaf-like α-Fe_2O_3 microparticles were synthesized via a facile template-free hydrothermal method, and their morphologies were characterized by X-ray diffraction, energy dispersive spectrometry, scanning electron microscope, and transmission electron microscope. Electrochemical characterization assays revealed that the hybrid film modified electrode had remarkable synergistic effects of the large accessible surface area and high electrical conductivity of semiconductive Fe_2O_3, and the good film stability of CS. Based on the rich amino groups on CS, the CS-Fe_2O_3 hybrid film was employed as a functional matrix for probe DNA immobilization using terephthalaldehyde (TPA) as a bifunctional arm-linker. The hybridization capacity of the developed biosensor was evaluated with electrochemical impedance spectroscopy (EIS) using $[Fe(CN)_6]^{3-/4-}$ as the indicating probe. A wide dynamic detection range from 1.0×10^{-14} to 1.0×10^{-10} M with ultralow detection limit of 5.6×10^{-15} M was achieved for the target DNA. The hybridization selectivity experiments further revealed that the biosensor could discriminate fully complementary sequences from one-base mismatched, three-base mismatched, and non-complementary sequences. Moreover, the biosensor showed the advantage of good regeneration ability and reproducibility.

Keywords

Fern leaf-like α-Fe_2O_3; Chitosan; Terephthalaldehyde; DNA biosensor; Hybridization

1. Introduction

In the past two decades, considerable efforts have been made to develop rapid, simple, and highly specific detection of DNA sequence due to its potential applications in many areas, such as gene identification, molecular diagnostic, drug screening, forensic science, environmental protection (Liu et al. 2012; Sassolas et al. 2008). Among various approaches of DNA detection, electrochemical methods attract significant attention owing to their advantages of simplicity, reliability, sensitivity, and selectivity as well as compatibility with microfabrication technology (Zhang et al. 2008; Chen et al. 2010). The critical step for the fabrication of DNA biosensor was to construct a well-defined functional matrix for effective immobilization of probes single-stranded DNA (ssDNA). Recent developments in nanomaterials and nanotechnologies provide great opportunities to enhance the immobilization effect of the probe DNA on the transducer interface (Zamborini et al. 2012; Walcarius et al. 2013； Du et al. 2009). For example, the large surface area effect is benefit to increase the immobilization amounts of the capture probe DNA (Zamborini et al. 2012; Walcarius et al. 2013), and the high electrocatalytic activities of some nanomaterials show great promising to enhance the signal intensity as well as sensitivity of the biosensor (Du et al. 2009).

Semiconductive nano-scaled metal oxides are one of the most popular materials used in electrochemical biosensors due to their high electrical conductivity, good biocompatibility, and easy preparation method (Noorbakhsh and Salimi 2011; Mathur et al. 2009). Hematite (α-Fe_2O_3) is one of the most stable iron oxide with n-type semiconducting properties with an indirect band gap of 2.2 eV at ambient conditions (Xiong et al. 2006). It has been extensively studied in areas of magnetic recording media, catalysts, pigments, electrode materials, gas sensors, optical devices, and electromagnetic devices, etc. (Sharma et al. 2013; Jiao and Wang 2013； Zhang et al. 2013). Due to its high stability and excellent electrical conductivity, it has also been used as electrode material for electrochemical sensing analysis of glucose (Cao and Wang 2011), deferoxamine (Heli et al. 2010), and folic acid (Maiyalagan et al. 2013).

On the other hand, the immobilization method of ssDNA probe onto the transducer surface also plays a critical role to affect the performance of a biosensor, including the stability,

reproducibility, regeneration ability, and sensitivity (Wang et al. 2013; Bonanni and Pumera 2011). In all the developed strategies, the covalent binding method receives considerable interesting because this method provides a stable detection layer preventing nucleic acids desorption from the electrode surface (Ligaj et al. 2006). Moreover, the covalent attachment of probe DNA via 3' or 5' terminal position usually results in a high hybridization efficiency, because the loading density, structural flexibility and orientation control of the ssDNA probe could be well assured by this way (Sassolas et al. 2008). The dialdehyde reagents based cross-linking reaction is a popular reaction type in biological conjugation, owing to its high reaction efficiency, mild reaction condition, and riskless by-products (H_2O). Moreover, through using multiplex atomic dialdehyde reagents as the cross-linker, the ssDNA chains could be kept away from the solid-phase electrode surface, which is valuable for the promotion of the hybridization efficiency of a biosensor (Wang et al. 2011). Glutaraldehyde (GTD) is a typical reactive dialdehydes reagent that has been often used as a fixative or cross-linker in biosensor fabrications (Prabhakar et al. 2008; Tembe et al. 2008; Devi et al. 2012; Yildirim et al. 2012). However, its excellent flexibility might lead to the complete cross-linking of both ends to the interface, thereby resulted in the absence of free aldehyde group to further react with the biological molecules (Wang et al. 2011). In contrast, another dialdehydes reagent of terephthalaldehyde (TPA) with a rigid phenyl group shows less flexibility than GTD, which make it having the higher efficiency to graft the biomolecules as a cross-linker (Khan et al. 1996).

In this work, the fern leaf-like Fe_2O_3 microparticles were synthesized hydrothermally using $K_3Fe(CN)_6$ as the raw materials. Then a well-dispersed solution containing Fe_2O_3 and chitosan (CS) was prepared, and cast on a glassy carbon electrode (GCE) to achieve CS-Fe_2O_3 hybrid modified electrode. Electrochemical assays showed that the electrode had high stability, large accessible surface area, and high electro-catalytic activity due to the synergistic effect of Fe_2O_3 and CS. The abundant amino groups on CS were first covalently coupled with one aldehyde group of TPA, and followed by, the residual aldehyde group on the other end of TPA was further reacted with the modified amino on the probe ssDNA. Thus, a novel DNA biosensor was constructed (Fig. 1). This highly conductive biosensor was further applied for the sensitive impedance detection of the DNA sequences, and the obtained results showed that a wide linear range from 1.0×10^{-14} M to 1.0×10^{-10} M with a low detection limit of 5.6×10^{-15} M was achieved for the target DNA, which

3

opens a new way for the construction of high-performance DNA biosensor.

<Here is Fig. 1>

Experimental

2.1. Chemicals and instruments

Tris (hydroxymethyl) aminomethane (Tris), CS and TPA were purchased from Aladdin Reagent Co., Ltd (China). Sodium borohydride ($NaBH_4$) was supplied by Shanghai Chemical Reagent Co., Ltd (China). Ethylenediaminetetraacetic acid (EDTA), $K_3Fe(CN)_6$ and $K_4Fe(CN)_6$ were provided by Xilong Chemical Co., Ltd (China). The other chemicals were of analytical reagent grade and obtained commercially. All the solutions were prepared with double-distilled water (DDW).

The 21-base synthetic oligonucleotides were purchased from Shanghai Sangon Bioengineering Co., Ltd (China). Their base sequences were as follows:

- Capture probe sequence (S1): 5′-NH_2-GGC AAC CTC GGA GAC TTA CGC-3′
- Complementary sequence (S2): 5′-GCG TAA GTC TCC GAG GTT GCC-3′
- One-base mismatched sequence (S3)：5′-GCG TAA GTC TCC GAG GTC GCC-3′
- Three-base mismatched sequence (S4)：5′-GCG TAA ATC CCC GAG GTC GCC-3′
- Non-complementary sequence (S5)： 5′-TCT AAC CTC GGA GAC TTA CGC-3′

Stoke solutions (10 μM) of all oligonucleotides were prepared with TE buffer solution (10 μM Tris-HCl, 1.0 mM EDTA, pH 8.0) and kept frozen.

The size and morphology of the synthesized samples were characterized by scanning electron microscopy (SEM, NoVa^{TM} Nano SEM 430, FEI Company) and transmission electron microscopy (TEM, Tecnai G20, FEI Company). X-ray powder diffraction was carried out on an X'pert PRO X-ray diffractometer (XRD, D8 Advance, Bruker Company) with Cu Kα radiation (λ=1.54056 Å) operating at 40 kV and 30 mA. The electrochemical experiments were measured on a CHI 650D electrochemical workstation (Shanghai CH Instrument Company) with the conventional three electrode system consisted of bare or modified glassy carbon electrode (GCE) as working electrode, Ag/AgCl/(3 M) as reference electrode and platinum wire as auxiliary electrode.

4

2.2. Preparation of the fern leaf-like Fe_2O_3

The Fe_2O_3 was synthesized according to a template-free solvothermal method using $K_3Fe(CN)_6$ as the raw material. Briefly, 0.30 g $K_3Fe(CN)_6$ was dissolved in 48 mL DDW and the pH value was adjusted to 8.0 with 0.1 M ammonia solution. Then the solution was transferred into a stainless steel autoclave (100 mL) of 80% capacity of the total volume, and heated at 150 °C for 48 h. After reaction, the autoclave was allowed to cool at room temperature. The red precipitates were then collected carefully and washed with ethanol and DDW for several times. After dried under vacuum at 60 °C, the products of Fe_2O_3 were obtained.

2. 3. Fabrication of the DNA biosensor

1.0 mg mL^{-1} CS solution was firstly prepared by dissolving 0.001 g of chitosan in 1 mL 1.0% (V/V) acetic acid, and then mixed with 1 mL 1 g L^{-1} Fe_2O_3 aqueous dispersion. Through ultrasonication for 1 h, a uniform brown solution was obtained, which was recorded as CS-Fe_2O_3. Prior to modification, the GCE surface was polished with 1.0, 0.3 and 0.05 μm alumina slurries on a cotton cloth sequentially, and then ultrasonically cleaned in ethanol and water for 5 min, respectively. Followed by, 10 μL of the prepared CS-Fe_2O_3 solution was cast on the pre-treated GCE and allowed to dry at room temperature. After the modified electrode was carefully rinsed with DDW to remove the loosely attached CS-Fe_2O_3, the modified electrode (CS-Fe_2O_3/GCE) was obtained. The modified electrode was then immersed into 30 mM aqueous solution of TPA for 1 h to obtain the TPA modified electrode (TPA/CS-Fe_2O_3/GCE). To further immobilize the probe DNA, the TPA/CS-Fe_2O_3/GCE was incubated in 1.0 μM S1 for 3 h, which was followed by immersing into 0.1 μM $NaBH_4$ solution for 40 min to convert the C=N bond to the more stable C-N bond (Walt and Agayn 1994). After rinsing with TE buffer solution, the probe DNA modified electrode (S1/TPA/CS-Fe_2O_3/GCE) was obtained.

2.4. Hybridization and electrochemical measurements of the biosensor

The hybridization reaction was performed by incubating S1/TPA/CS-Fe_2O_3/GCE into 180 μL analyte solution (S2, S3, S4 or S5) with desired concentration for 40 min at 42 ^oC, and then rinsed with TE buffer to remove the nonspecifically adsorbed DNA.

The cyclic voltammetry (CV) and electrochemical impendance spectra (EIS) were carried out in 1.0 mM $[Fe(CN)_6]^{3-/4-}$ (1:1) and 0.1 M KCl mixture. The scan rate in CV was 100 mV s^{-1} and

5

the potential window was between +0.6 V and -0.2 V. The EIS was collected at a potential of +0.172 V in the frequency range from 10^4 Hz to 0.1 Hz with the voltage amplitude of 5 mV. The reported result for every electrode in this paper was the mean value of three parallel measurements.

2. Results and discussion

3.1. Structure and morphology characterization of the Fe_2O_3 microparticles

<Here is Fig. 2>

The phase composite and structure of the synthesized products were examined by XRD, and the result was displayed in Fig. 2A. As seen, all the diffraction peaks were strong and sharp, indicating good crystallization of the products. By comparison with the JCPDS Card no. 89-0598, all the diffraction peaks could be well indexed as the rhombohedral phase (space group R-3c) of α-Fe_2O_3 with cell constants of a =5.038 Å and c =13.776 Å. EDS analysis (Fig. 2B) further confirmed that the prepared samples were consisted of Fe and O as no other element was detected. The atomic ratio of Fe/O was calculated to be 0.64, which was very close to the composition of Fe_2O_3. All these results indicated that the α-Fe_2O_3 had been successfully synthesized. The morphology of the synthesized Fe_2O_3 was characterized by SEM and TEM. Fig. 2C displayed the typical SEM image of the Fe_2O_3 at the lower magnifications, in which many uniform and independent Fe_2O_3 dendrites were observed. From the high magnification SEM image as showed in Fig. 2D, one could further observe that each dendrite was consisted by a pronounced stem with two groups of highly symmetric and parallel branch, which was very similar to a natural fern leaf as showed in inset of Fig. 2D. In addition, the angle between the branch and the main stem was determined to be about 48º. The ordered and uniform feature meant that the growth of the products was diffusion controlled globally, but locally accomplished through oriented attachment (Thirumalairajan et al. 2013). Fig. 2E and Fig. 2F showed the TEM and HRTEM of the Fe_2O_3. From the TEM, it could be observed that the stem in length was in the range of from 400 nm to 2 μm and 7-10 nm in width. From the HRTEM image (Fig. 2F), the lattice fringes could be observed clearly and the lattice spacing was determined to be 0.251 nm, corresponding to the (110) plane of α-Fe_2O_3 (Shi et al. 2013). This confirms the single-crystal structure of nanosized branch of the fern-like Fe_2O_3.

3.2. Electrochemical characterization of Fe_2O_3 modified electrode

6

Electrocatalytic property of the synthesized Fe_2O_3 was characterized by CV and EIS using $[Fe(CN)_6]^{3-/4-}$ ions as the redox probe. Fig. S1A in the Supporting Information shows the CVs of $[Fe(CN)_6]^{3-/4-}$ on bare GCE (curve a), Fe_2O_3/GCE (curve b), CS/GCE (curve c) and CS-Fe_2O_3/GCE (curve d). As well seen, a couple of reversible redox peaks was observed on bare GCE (curve a). While on CS/GCE, the redox peak intensity was decreased significantly and the peak-to-peak separation was enlarged obviously, indicating that the CS modified on the electrode surface had blocking effect to the electrochemical reaction of $[Fe(CN)_6]^{3-/4-}$ due to its inferior electric conductivity. While on Fe_2O_3/GCE the redox peak was increased a little compared with CS/GCE, but it was still smaller than that on bare GCE, suggesting that the single-component of Fe_2O_3 microparticles could not improve the electrochemical response of the electrode. It was interesting that on the CS-Fe_2O_3/GCE, significantly increased redox peak of $[Fe(CN)_6]^{3-/4-}$ was observed (curve d), which indicated that the composite film of CS-Fe_2O_3 had great influence on the improvement of the electrochemical property of the electrode. This could be explained by the synergistic effect of excellent electric conductivity of Fe_2O_3 and good charge penetration property of CS film. In addition, according to the reduction peak current of $[Fe(CN)_6]^{3-}$ and the following Randles-Sevcik equation (Xiao et al. 2008).

$$I_{pc}= (2.69\times10^5)n^{3/2}AD^{1/2}Cv^{1/2}$$

where I_{pc} is the reduction peak current (A), n the electron transfer number, D the diffusion coefficient ($cm^2\ s^{-1}$), C the concentration (M) and v the scan rate ($V\ s^{-1}$), the accessible surface area (A) of bare GCE, Fe_2O_3/GCE, CS/GCE and CS-Fe_2O_3/GCE were calculated to be 0.14 cm^2, 0.10 cm^2, 0.05 cm^2 and 0.42 cm^2, respectively, which suggested that the presence of Fe_2O_3 microparticles in composite film could markedly increase the electroactive surface area of the sensing interface due to their size effect.

The electro-catalytic property of Fe_2O_3 was further characterized by EIS, which has been regarded as a sensitive method to probe the electron transfer resistance (R_{et}) of an interface. In the EIS, the semicircle portion observed at high frequencies corresponds to the electron transfer limiting process, and the interfacial R_{et} can be directly determined by the diameter of the semicircle. Fig. S1B in the Supporting Information shows the typical EIS in the form of Nyquist diagrams of different electrodes in $[Fe(CN)_6]^{3-/4-}$. One could observe that the cleaned bare GCE behaved as an ideal conductor as determined from the small R_{et} value of 4.6×10^2 Ω (curve a).

7

While on Fe_2O_3/GCE and CS/GCE, the R_{et} values increased to 1.6×10^3 Ω (curve b) and 2.1×10^3 Ω (curve c), respectively, indicating the coating of single-component of Fe_2O_3 or CS on the electrode surface could not improve the electron transfer rate. However, the R_{et} value on CS-Fe_2O_3/GCE was significantly decreased to 2.5×10^2 Ω (curve d), which was even lower than the bare GCE. This variation displayed a strong proof that the nanocomposite of CS-Fe_2O_3 had obvious electrocatalytic effect. The low R_{et} and large accessible surface of CS-Fe_2O_3/GCE demonstrated that the nanocomposite could be used as a high-performance platform for electrochemical biosensing analysis.

3.3. DNA immobilization on CS-Fe_2O_3/GCE using TPA as cross-linker

<Here is Fig. 3>

In this work, the covalent immobilization of probe DNA on the surface of CS-Fe_2O_3/GCE was realized through using TPA as a facile arm-like cross-linker, and the process was also characterized by CV and EIS techniques. The results were displayed in Fig.3. It was found that the redox probe of $[Fe(CN)_6]^{3-/4-}$ on TPA/CS-Fe_2O_3/GCE were decreased obviously (curve b) after the CS-Fe_2O_3/GCE was reacted with TPA, which could be attributed to the hindering of the electron transfer of $[Fe(CN)_6]^{3-/4-}$ by the increased film thickness. This also testified that the TAP molecules had been grafted to CS-Fe_2O_3/GCE via the facile aldehyde-amino condensation reaction. After the TPA confined electrode (i.e., TPA/CS-Fe_2O_3/GCE) was further incubated in probe DNA (S1) solution, the redox peak was further decreased remarkably (curve c), suggesting that the probe DNA had been successfully anchored on TPA/CS-Fe_2O_3/GCE and the immobilized DNA blocked the electron transfer of $[Fe(CN)_6]^{3-/4-}$ through the electrostatic repulsion and the steric hindrance effect (Park and Park 2009). The EIS results (inset of Fig. 3) were in good agreement with those from above CV studies. Both results of EIS and CV indicated that the DNA biosensor had been fabricated successfully.

3.4. Optimization of the biosensor preparation

In order to obtain the optimal sensing performance of the sensor, the influence of the ratio of Fe_2O_3 microparticles to CS in the composite membrane was optimized by CV assays. Fig. S2 in the Supporting Information shows the CVs of 1.0 mM $[Fe(CN)_6]^{3-/4-}$ with 0.1 M KC1 at GCE

8

before (curve a) and after modification with dispersion of Fe_2O_3 solution (1.0 g L^{-1}) and CS (1.0 g L^{-1}) at volume ratio of 1:1 (curve b), 1:2 (curve c) and 1:3 (curve d). As seen, all the modified electrodes had the higher redox peaks than bare GCE (curve a), suggesting the electrocatalysis of the as-prepared nanocomposite. Moreover, in all the modified electrodes, the largest redox peak of $[Fe(CN)_6]^{3-/4-}$ was appeared at the ratio of 1:2, suggesting that the Fe_2O_3 to CS at this ratio had the best electrocatalysis effect. Therefore, the mixture solution of Fe_2O_3 to CS with the volume ratio of 1:2 was chosen as the optimal modification solution.

The reaction time of TPA with CS-Fe_2O_3/GCE was also investigated. It was found that the R_{et} values of the assembled electrodes increased with the prolonging of the incubation time of CS-Fe_2O_3/GCE in TPA solution. When the time was upon 1 h, the R_{et} value became a constant, indicating that a saturation state of TPA film had been formed on the electrode surface. Therefore, 1 h was chose as the optimal assembly time for preparation of the TPA modification layer.

The immobilization time of S1 on TPA/CS-Fe_2O_3/GCE was also optimized, and the result showed that the R_{et} value of the modified electrode increased with the increase of reaction time of TPA/CS-Fe_2O_3/GCE in probe solution. When the time was up to 3 h, the value of R_{et} reached to the largest value, implying a binding equilibrium between probe DNA and TPA on the electrode surface. So, 3 h was used as the immobilization time of S1. In addition, to further determine the immobilization effect, the surface density of the probe DNA was investigated in Tris-HCl buffer by chronocoulometric (CC) method using $Ru(NH_3)_6^{3+}$ as the electrochemical probe. Fig. S3 in the Supporting Information shows the typical CC curves of S1/TPA/CS-Fe_2O_3/GCE in Tris-HCl without (curve a) and with 50 μM $[Ru(NH_3)_6]^{3+}$ (curve b), and the value of the probe DNA surface density was calculated to be 8.83×10^{12} molecules cm^{-2} according to the method reported by Steel et al. (Steel et al. 1998). It had been reported that the high density of probe DNA usually caused steric and electrostatic hindrance for the target DNA, leading to low hybridization efficiency of the biosensor (Zhang, et al. 2006); however, the over-low surface density will reduce the capture amount of the biosensor to the target DNA. Therefore, the surface density played a critical role to affect the performance of a DNA biosensor. From the literature (Zhang, et al. 2006), the obtained DNA density of 8.83×10^{12} molecules cm^{-2} in this work belonged to a medium-level density, which might be popular to achieve an equilibrium between hybridization efficiency and capture amount of target DNA.

9

3.5. Analytical performance of the biosensor

<Here is Fig. 4>

The analytical performance of the biosensor was also investigated through EIS. Fig. 4 shows the Nyquist plots of S1/TPA/CS-Fe_2O_3/GCE hybridization with different concentrations of S2. It was observed that the R_{et} values increased accordingly with the increase of S2 concentration (C_{S2}) in the hybridization solution. When the difference of R_{et} (ΔR_{et}) value on the biosensor before and after hybridization was used as the sensing signal, it was found that the ΔR_{et} values were well proportional to the logarithm of C_{S2} (lg C_{S2}) in the range from 1.0×10^{-14} M to 1.0×10^{-10} M. The linear regression equation was $\Delta R_{et}/k\Omega$ = 0.5563(±0.0040) lg (C_{S2}/M) + 8.68 (±0.51) with the correlation coefficient (r) of 0.9963 (Inset of Fig. 4). A low detection limit of 5.6×10^{-15} M was estimated at a signal-to-noise (S/N) ratio of 3. It was noticeable that such an analytical performance was obtained under the condition of immobilizing probe DNA at electrode surface for 3 h, with the probe density of 8.83×10^{12} molecules cm^{-2}. In order to probe whether such a condition is optimal to construct the biosensor with the best analytical performance, a control electrode with shorter immobilization time (2 h) of probe DNA on TPA/CS-Fe_2O_3/GCE was fabricated, and its hybridization performance was also evaluated by EIS (Fig. S4 in the Supporting Information). Through the result, it was obtained that the linear range of ΔR_{et} versus lg C_{S2} was from 1.0×10^{-12} M to 1.0×10^{-8} M with the detection limit of 4.7×10^{-13} M. This result confirmed that the biosensor with the probe immobilization time of 3 h (8.83×10^{12} molecules cm^{-2} of probe density) had the better hybridization response.

The analytical results of the proposed biosensor were also compared with the other metal oxide-based electrochemical biosensors, and the results were listed in Table S1 in the Supporting Information. Through the comparison, it could be concluded that the sensing platform presented in this work had the higher sensitivity for target DNA detection, which might be assigned to the synergic effect of the high conductivity and large surface area of CS-Fe_2O_3 film.

The selectivity of this DNA biosensor was further evaluated by hybridization with different DNA sequences. The obtained Nyquist diagrams were shown in Fig. 5, and the corresponding R_{et} value on each hybridized electrode was depicted as histogram in inset of Fig. 5. One could observe that the value of R_{et} showed negligible variation after S1/TPA/CS-Fe_2O_3/GCE was hybridized with the non-complementary sequence of S5 (curve b), indicating that the hybridization reaction and

10

the non-specific absorption of non-complementary DNA on the electrode surface were not happened. However, after the biosensor was hybridized with the fully complementary sequence of S2, the obtained R_{et} value increased extremely (curve e), suggesting that hybridization reaction was achieved at the electrode. In addition, when the biosensor was hybridized with the single-base mismatched sequence of S3 (curve d) or three-base mismatched sequence of S4 (curve c), the increase of the R_{et} value was much smaller than that obtained from the case of the hybridization with the S2. Meanwhile, the mismatched degree of on S4 and S3 could also be recognized via comparing the difference of the ΔR_{et} values on these two electrodes. These results demonstrated that the developed DNA biosensor displayed a very high selectivity for the hybridization detection

<Here is Fig. 5>

3.6. Stability and reproducibility of the DNA biosensor

The reusability of the DNA biosensor was extremely important for practical application such as clinical diagnoses and biological monitoring, which was dependent on the stability and regeneration ability of the biosensor. In this work, it was found that when the fabricated biosensor of S1/TPA/CS-Fe_2O_3/GCE was stored at 4 ^oC for 10 days, and then measured with EIS in $[Fe(CN)_6]^{3-/4-}$, only a change of 3.7% in the R_{et} response was observed as compared with the initial test, which indicated the good stability of the biosensor. The regeneration of the DNA biosensor was conducted by immersing the in hot water (85 ^oC) for 5 min, and then washed with DDW, followed by storing at 4 ^oC. As Fig. S5 in the Supporting Information shows, after five runs of regeneration, the R_{et} values almost recovered to the initial value, which reveals a remarkable regeneration ability of the developed DNA biosensor. Such a high regeneration ability of the biosensor can be ascribed to the high stability of the CS-Fe_2O_3 composite film and the firm covalent bonding of probe DNA with the immobilization matrix. Reproductivity of the biosensor was monitored by five parallel-made DNA biosensors to detect 1.0×10^{-10} M target DNA, and the results showed that a relative standard deviation (RSD) of 8.89% (n = 6) was obtained, suggesting a high reproducibility of the constructed DNA biosensor.

3.7. Feasibility of the biosensor in complex sample

In order to investigate the feasibility of the developed DNA biosensor in complex matrixes, 1.0×10^{-11} M pure complementary DNA (S2) and non-complementary DNA (S5) were separately added into two clinical serum samples diluted (10% (v/v)) with TE buffer, and then analyzed by

11

the developed biosensor. The EIS results were displayed in Fig. S6 in the Supporting Information. From the results, it was observed that compared with the unhybridized biosensor (curve a), only small change was occurred when non-complementary DNA was tested (curve b). However, a significant increase of R_{et} was observed for the complementary DNA sample, demonstrating that the developed biosensor remained good recognition ability in the complex sample. The recovery was calculated to be 103.6%, suggesting the significant feasibility of the biosensor in practice.

4. Conclusions

In this paper, fern leaf-like α-Fe_2O_3 microparticles were synthesized through a simple solvothermal method. Then the reagent of terephthalaldehyde was used as an arm linker to covalently immobilize the probe sequence to the GCE surface modified with the fern leaf-like Fe_2O_3 microparticles and chitosan composite. The existence of Fe_2O_3 in the composite film greatly enhances the electron conductivity of the biosensor, and chitosan provides abundant amino groups for covalent bonding of the arm molecules of terephthalaldehyde and probe ssDNA. The developed biosensor was successfully applied to the electrochemical impedance detection of DNA hybridization and the experimental results showed highly sensitivity, good stability and excellent reproductivity. Moreover, the reported biosensor achieved impressive selectivity with successful discrimination of the target DNA from mismatch sequences. Therefore, the proposed method may present a promising strategy for constructing high-performance electrochemical biosensors for DNA analysis in the future.

5. Acknowledgments

The work is supported by the National Natural Science Foundation of China (No. 21275127), Program for New Century Excellent Talents in Fujian Province University (No. JA12204), and Scientific Research Fund of Fujian Provincial Education Department (No. JA14195).

References

Bonanni, A., Pumera, M., 2011. ACS Nano. 5, 2356-236.

Cao, X., Wang, N., 2011. Analyst 136, 4241-4246.

Chen, J., Zhang, J., Yang, H., Fu, F., Chen, G., 2010. Biosens. Bioelectron. 26, 144-148.

Devi, R., Yadav, S., Pundir, C.S., 2012. Colloid Surf. A-Physicochem. Eng. Asp. 394, 38-45.

Du, P., Li, H., Mei, Z., Liu, S., 2009. Bioelectrochemistry 75, 37-43.

Heli, H., Majdi, S., Sattarahmady, N., Parsaei, A., 2010. J. Solid State Electrochem. 14,

12

1637-1647.

Jiao, H., Wang, J., 2013. J. Alloys Compd. 577, 402-408.

Khan, Y.M., Starling, A.P., East, J.M., Lee, A.G., 1996. Biochem. J 317, 439-445.

Ligaj, M., Jasnowska, J., Musiał, W.G., Filipiak, M., 2006. Electrochim. Acta 51, 5193-5198.

Liu, A., Wang, K., Weng, S., Lei, Y., Lin, L., Chen, W., Lin, X., Che, Y., 2012. Trends Anal. Chem. 37, 101-111.

Maiyalagan, T., Sundaramurthy, J., Suresh Kumar, P., Kannan, P., Opallo, M., Ramakrishna, S., 2013. Analyst 138, 1779-1786.

Mathur, S., Erdem, A., Cavelius, C., Barth, S., Altmayer, J., 2009. Sens. Actuators, B: chem. 136, 432-437.

Noorbakhsh, A., Salimi, A., 2011. Biosens. Bioelectron. 30, 188-196.

Park, J.Y., Park, S.M., 2009. Sensors (Basel). 9, 9513-9532.

Prabhakar, N., Arora, K., Singh, H., Malhotra, B.D., 2008. J. Phys. Chem. B. 112, 4808-4816.

Sassolas, A., Leca-Bouvier, B.D., Blum, L.J., 2008. Chem. Rev. 108, 109-139.

Sharma, R., Agrawal, V.V., Srivastava, A.K., Govind, Nain, L., Imran, M., Kabi, S.R., Sinha, R.K., Malhotra, B.D., 2013. J. Mater. Chem. B 1, 464-474.

Shi, G., Zhang, K., Zhou S., Zhang, Q., 2013. Mater. Lett. 107, 228-230.

Steel, A.B., Herne, T.M., Tarlov, M.J., 1998, Anal. Chem. 70, 4670-4677.

Tembe, S., Kubal, B.S., Karve, M., D'Souza, S.F., 2008. Anal. Chim. Acta. 612, 212-217.

Thirumalairajan, S., Girija, K., Ganesh, V., Mangalaraj, D., Viswanathan, C., Ponpandian, N., 2013. Cryst. Growth Des. 13, 291-302.

Walcarius, A., Minteer, S.D., Wang, J., Lin, Y., Merkoçi, A., 2013. J. Mater. Chem. B 1, 4878-4908.

Walt, D.R., Agayn, V.I., 1994. TrAC, Trends Anal. Chem. 13, 425-430.

Wang, Q., Ding, Y., Gao, F., Jiang, S., Zhang, B., Ni, J., Gao, F., 2013. Anal. Chim. Acta 788, 158-164.

Wang, Q., Zhang, B., Lin, X.Q., Weng, W., 2011. Sens. Actuators, B: chem. 156, 599-605.

Xiao, F., Zhao, F., Li, J., Liu, L., Zeng, B., 2008. Electrochim. Acta 53, 7781-7788.

Xiong, G., Joly, A.G., Holtom, G.P., Wang, C., McCready, D.E., Beck, K.M., Hess, W.P., 2006. J. Phys. Chem. B 110, 16937-16940.

13

Yildirim, N., Long, F., Gao, C., He, M., Shi H.C., Gu, A.Z., 2012. Environ. Sci. Technol. 46, 3288-3294.

Zamborini, F.P., Bao, L., Dasari, R., 2012. Anal. Chem. 84, 541-576.

Zhang, J., Song S., Zhang L., Wang L., Wu H., Pan D., Fan C., 2006. J. Am. Chem. Soc. 128, 8575-8580.

Zhang, L., Dong, W.F., Sun, H.B., 2013. Nanoscale 5, 7664-7684.

Zhang, W., Yang, T., Huang, D., Jiao, K., Li, G., 2008. J. Membr. Sci. 325, 245-251.

Figure captions

Fig. 1 Schematic illustration of preparation and hybridization of the DNA biosensor.

Fig. 2 XRD (A) and EDS (B) patterns of the synthesized Fe_2O_3. (C) Typical low magnification and (D) high magnification SEM images of the products. (E) Low magnification and (F) high resolution TEM images of the Fe_2O_3. Inset in (D) showed an electronic photo of natural fern leaf, and Inset in (E) is the TEM image of a single fern leaf-like Fe_2O_3 particles.

Fig. 3 Cyclic voltammograms and Nyquist diagrams (inset) of 1.0 mM $[Fe(CN)_6]^{3-/4-}$ with 0.1 M KC1 on CS-Fe_2O_3/GCE (a), TPA/CS-Fe_2O_3/GCE (b) and S1/TPA/CS-Fe_2O_3/GCE (c).

Fig. 4 Nyquist diagrams of 1.0 mM $[Fe(CN)_6]^{3-/4-}$ with 0.1 M KC1 at S1/TPA/CS-Fe_2O_3/GCE before (a) and after hybridization with 1.0×10^{-14} M (b), 1.0×10^{-13} M (c), 1.0×10^{-12} M (d), 1.0×10^{-11} M (e), 1.0×10^{-10} M (f), 1.0×10^{-9} M (g) S2. Inset shows the linear plot of ΔR_{et} values versus the logarithm of S2 concentrations (lg C_{S2}).

Fig. 5 Nyquist diagrams and the corresponding histogram (Inset) of R_{et} values on the biosensor before (a) and after hybridization with 1.0×10^{-9} M non-complementary sequence of S5 (b), three-base mismatched sequence of S4 (c), single-base mismatched sequence of S3 (d) and complementary sequence of S2 (e).

Highlights

- Fern leaf-like α-Fe_2O_3 microparticles was synthesized via a facile template-free method.
- Fe_2O_3 presents a large accessible surface area and high electrical conductivity.
- A DNA biosensor was fabricated using chitosan-Fe_2O_3 as matrix and terephthalaldehyde as arm-linker.
- High sensitivity and selectivity were achieved by the biosensor.

14

Figures

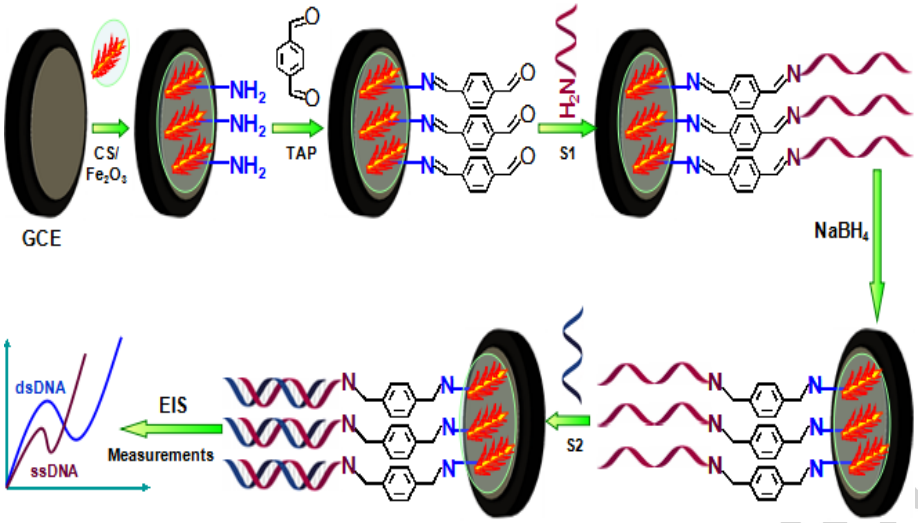

Fig. 1

17

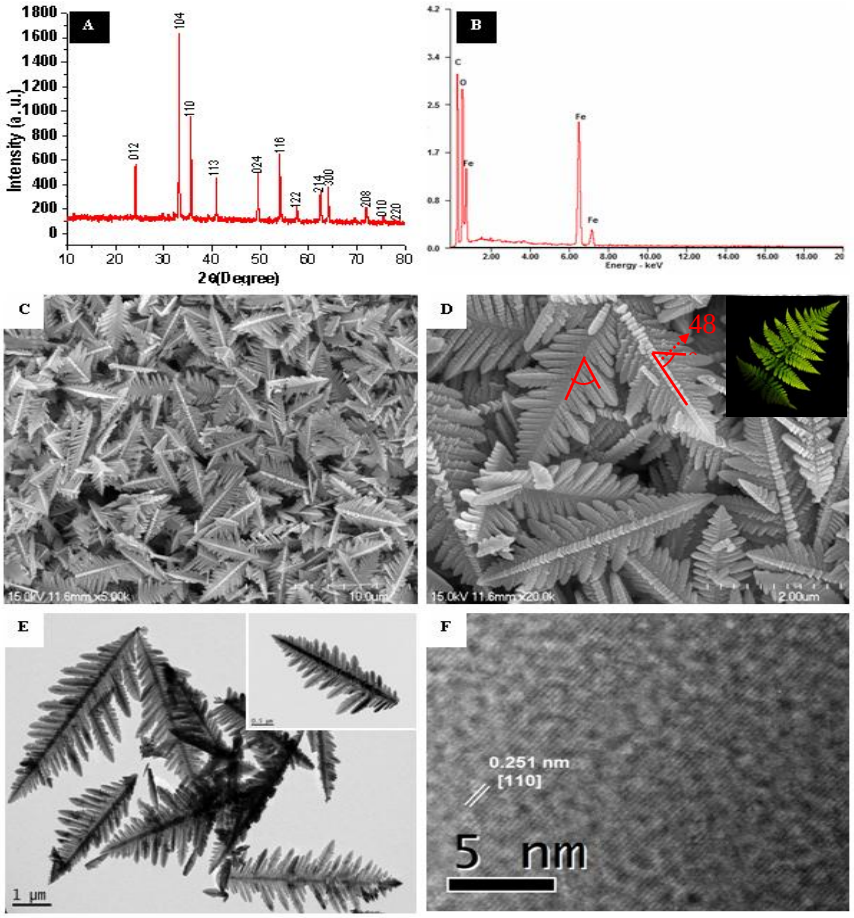

Fig. 2

18

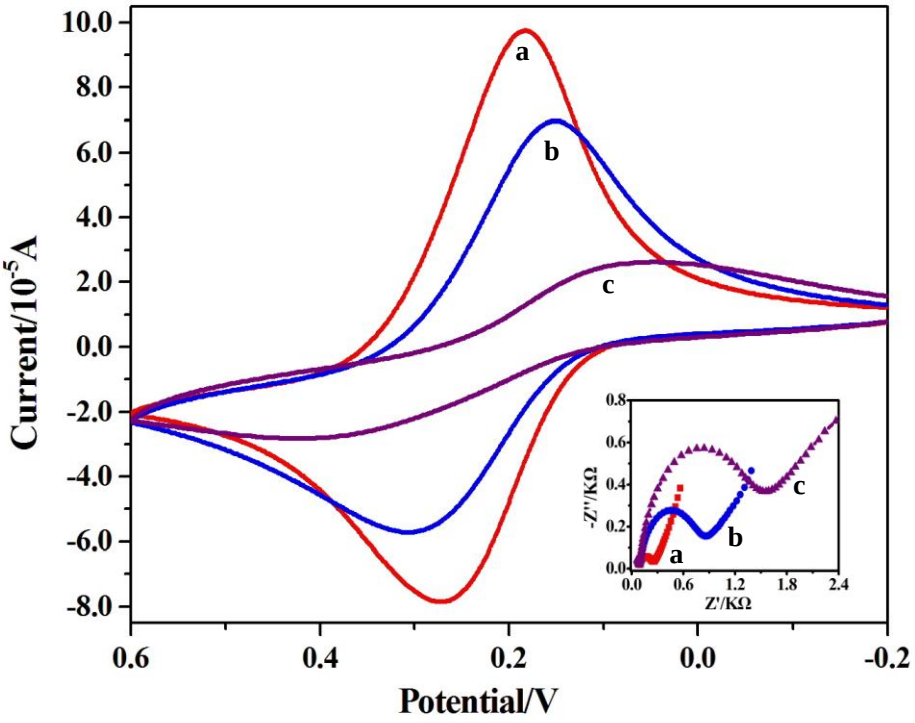

Fig. 3

19

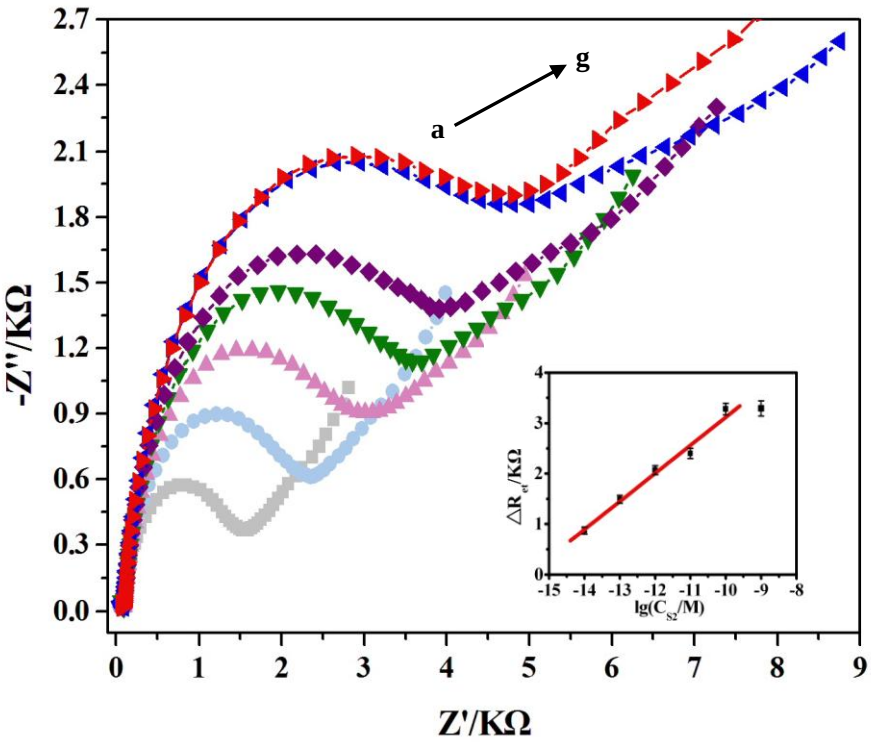

Fig. 4

20

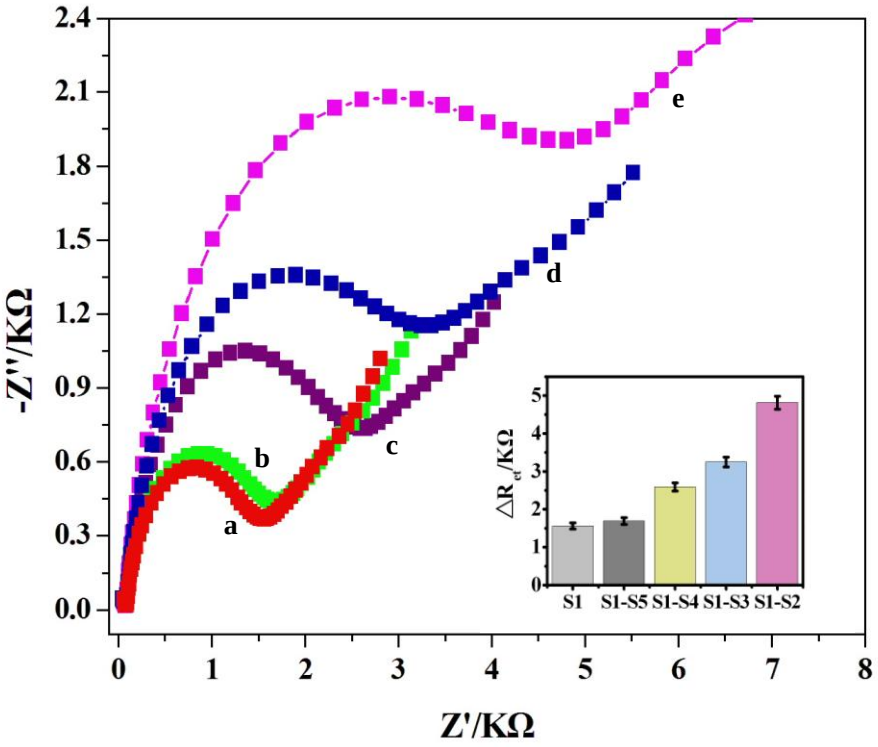

Fig. 5

21